PCT WORLD INTELLECTUAL PROPERTY ORGANIZATION
International Bureau

INTERNATIONAL APPLICATION PUBLISHED UNDER THE PATENT COOPERATION TREATY (PCT)

(51) International Patent Classification 6 : G01N	A2	(11) International Publication Number: **WO 98/52011**
		(43) International Publication Date: 19 November 1998 (19.11.98)

(21) International Application Number: PCT/US98/09775

(22) International Filing Date: 14 May 1998 (14.05.98)

(30) Priority Data:
60/047,008 14 May 1997 (14.05.97) US

(71) Applicant *(for all designated States except US)*: EMORY UNIVERSITY [US/US]; 1380 South Oxford Road, Atlanta, GA 30322 (US).

(72) Inventor; and
(75) Inventor/Applicant *(for US only)*: BROOKS, Kenneth, W. [US/US]; 31 Elan Way, Marietta, GA 30068 (US).

(74) Agents: PRATT, John, S. et al.; Kilpatrick Stockton LLP, Suite 2800, 1100 Peachtree Street, Atlanta, GA 30309–4530 (US).

(81) Designated States: AU, CA, JP, US, European patent (AT, BE, CH, CY, DE, DK, ES, FI, FR, GB, GR, IE, IT, LU, MC, NL, PT, SE).

Published
Without international search report and to be republished upon receipt of that report.

(54) Title: SYSTEMS AND METHODS FOR ANALYZING PHANTOM IMAGES

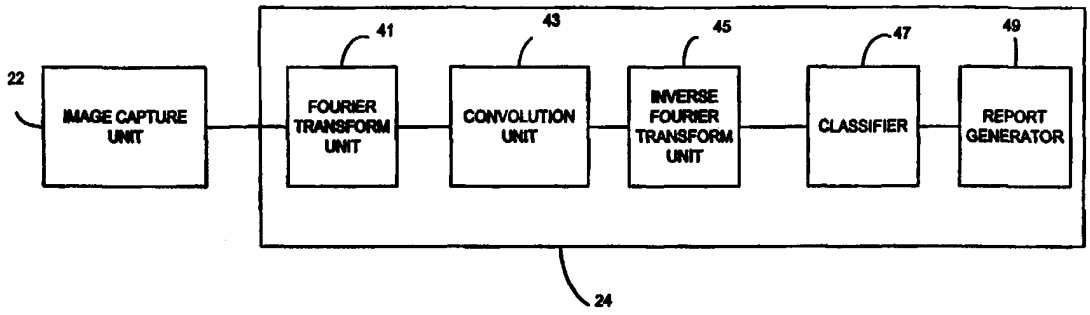

(57) Abstract

A significant metric in federal mammography quality standards is the phantom image quality assessment. A Mammography Quality Control System (MQCS) (20, 20') performs automated image analyses for the American College of Radiology (ACR) mammographic accreditation phantom (MAP) images. The MQCS (20, 20') uses a Fast Fourier Transform unit (41) for low–level processing combined with derivative filters for intermediate–level processing to provide translation and rotation independent localization of test objects in the MAP images. The MQCS (20, 20') uses a Bayesian classifier (47) using threshold contrast. The fifty percent visibility contrast thresholds established by the trained observer's responses were: fibrils 1.010; microcalcifications 1.156; and nodules 1.016. Using these values and given automated localization of test objects, the MQCS (20, 20') scores images with better consistency than the diagnostic physicists. The MQCS (20, 20') thus provides an operator independent, machine–based scoring of MAP images that is used to help eliminate the effect of observer variability.

FOR THE PURPOSES OF INFORMATION ONLY

Codes used to identify States party to the PCT on the front pages of pamphlets publishing international applications under the PCT.

AL	Albania	**ES**	Spain	**LS**	Lesotho	**SI**	Slovenia
AM	Armenia	**FI**	Finland	**LT**	Lithuania	**SK**	Slovakia
AT	Austria	**FR**	France	**LU**	Luxembourg	**SN**	Senegal
AU	Australia	**GA**	Gabon	**LV**	Latvia	**SZ**	Swaziland
AZ	Azerbaijan	**GB**	United Kingdom	**MC**	Monaco	**TD**	Chad
BA	Bosnia and Herzegovina	**GE**	Georgia	**MD**	Republic of Moldova	**TG**	Togo
BB	Barbados	**GH**	Ghana	**MG**	Madagascar	**TJ**	Tajikistan
BE	Belgium	**GN**	Guinea	**MK**	The former Yugoslav Republic of Macedonia	**TM**	Turkmenistan
BF	Burkina Faso	**GR**	Greece			**TR**	Turkey
BG	Bulgaria	**HU**	Hungary	**ML**	Mali	**TT**	Trinidad and Tobago
BJ	Benin	**IE**	Ireland	**MN**	Mongolia	**UA**	Ukraine
BR	Brazil	**IL**	Israel	**MR**	Mauritania	**UG**	Uganda
BY	Belarus	**IS**	Iceland	**MW**	Malawi	**US**	United States of America
CA	Canada	**IT**	Italy	**MX**	Mexico	**UZ**	Uzbekistan
CF	Central African Republic	**JP**	Japan	**NE**	Niger	**VN**	Viet Nam
CG	Congo	**KE**	Kenya	**NL**	Netherlands	**YU**	Yugoslavia
CH	Switzerland	**KG**	Kyrgyzstan	**NO**	Norway	**ZW**	Zimbabwe
CI	Côte d'Ivoire	**KP**	Democratic People's Republic of Korea	**NZ**	New Zealand		
CM	Cameroon			**PL**	Poland		
CN	China	**KR**	Republic of Korea	**PT**	Portugal		
CU	Cuba	**KZ**	Kazakstan	**RO**	Romania		
CZ	Czech Republic	**LC**	Saint Lucia	**RU**	Russian Federation		
DE	Germany	**LI**	Liechtenstein	**SD**	Sudan		
DK	Denmark	**LK**	Sri Lanka	**SE**	Sweden		
EE	Estonia	**LR**	Liberia	**SG**	Singapore		

SYSTEMS AND METHODS FOR ANALYZING PHANTOM IMAGES

FIELD OF THE INVENTION

This invention generally relates to systems and methods for analyzing phantom images and, more particularly, to systems and methods for analyzing phantom images for performing automated accreditation, such accrediting mammographic images for the American College of Radiology.

BACKGROUND OF THE INVENTION

The ability to acquire noninvasive images of a body, such as a human body, has proven to be invaluable to the medical community. Imaging techniques such as X-ray, Magnetic Resonance Imaging (MRI), ultrasonic imaging, radio-wave imaging, thermal imaging, and Computer Tomographic (CT) imaging allow precise images of a body to be taken and analyzed. These images have been used for a variety of purposes, such as in precisely locating tissues, detecting cancerous tissues, or detecting any medical anomaly. The above-mentioned imaging techniques and uses of the images are certainly not an exhaustive list and many other techniques and purposes for acquiring an image are known to those skilled in the art.

Mammography is one example of an imaging technique which is used to detect breast cancer. The first clinically useful mammography technique was developed in 1960 and studies were done in the late 1960's to determine whether regular screening with physical examination and mammography could reduce deaths from breast cancer. The use of mammography increased during the 1970's with the sponsorship of a breast cancer detection demonstration project by the American Cancer Society (ACS) and the National Cancer Institute (NCI). A concern about the adverse effects of the radiation from mammography led to a marked decline to the use of mammography at the end of the 1970's.

In the early 1980's, efforts were made to reduce radiation dosages received by a patient during a mammography screening. A joint federal-state program called Breast Exposure: Nationwide Trends (BENT) operated in most states to locate facilities giving excessively high radiation exposures and to assist them in reducing the exposures. As a result of the BENT program and also due to efforts in the industry to improve equipment and films, radiation doses began to decrease and concerns about radiation exposures in mammography had largely dissipated. During this time, the general purpose X-ray equipment was replaced with dedicated mammography units.

The reduction in mammography doses led to a new concern that the lower doses compromised image quality. A national study conducted in 1985 by the Food and Drug Administration (FDA) and State governments called the Nationwide Evaluation of X-ray Trends (NEXT) focused on the problems of image quality and radiation exposure. The NEXT program found that despite the employment of dedicated mammography equipment wide variations still existed in the quality of mammography and in the mammography dose at different mammography facilities. The NEXT program found that the image quality was not caused by the imaging equipment but rather due to poor techniques in operating the equipment. These problems in technique included improper film processing and improper use of image receptors.

The American College of Radiology developed the Mammography Accreditation Program (MAP) in an attempt to reduce variations in image quality between mammography facilities. The American College of Radiology also published Quality Control Manuals to guide radiologists, radiologic technologists, and medical physicists in providing quality mammography. The Quality Control Manuals place a heavy emphasis on processor quality control. Participation in MAP was voluntary, although most mammography facilities had enrolled by 1992. The Health Care Financing Administration (HCFA) also developed and imposed its own set of regulations as a condition for Medicare reimbursement. The Medicare

regulations were largely based on the American College of Radiology's MAP program, but did have some differences.

In 1992, Congress enacted the Mammography Quality Standards Act (MQSA) in order to ensure that all facilities providing Mammography were certified by the FDA. Prior to this time, the FDA regulated the mammography equipment but not the accrediting program. As a result, the quality of mammography still varied between facilities. Additionally, some non-accredited sites falsely claimed that they had accreditation status. The MQSA was therefore enacted in an effort to provide uniform high quality imaging by requiring all facilities to be certified and accredited.

An integral portion of the American College of Radiology (ACR) Mammography Accreditation Program (MAP) is the phantom image quality test. The phantom image quality test alone accounts for 25% of the MAP's failures and an additional 10% fail due to both the phantom image quality criterion and a clinical mammogram criterion. A phantom is a plastic device embedded with objects of varying materials and size that is used to evaluate image quality. The device is imaged as though it were a breast and an image score is determined by the number of objects picked up by the image. MAP phantoms contain clinically relevant test objects designed to represent typical breast pathologies: fibrils or "fibers," microcalcification groups or "specks," and nodules or "masses." The objects decrease in size and contrast sufficiently to demonstrate a visibility threshold using a typical clinical image technique and viewing apparatus. For certification, a facility's phantom image is analyzed independently by three American Board of Radiology (ABR) certified medical physicists who are experienced in mammography quality control and trained in reading phantom images. The criteria used by the readers has evolved to include a system of partial scores commensurate with the perceived object visibility as well as a system of deductions for image artifacts. The three independent object visibility net scores

are averaged and must demonstrate visibility for at least four fibers, three microcalcification groups, and three masses.

A requirement for using phantoms to monitor image quality is non-variable, consistent viewers. However, there are two sources of variability in the MAP process which could lead to inconsistent accreditation failure. First, the perceptive variability which exists among medical physicists which results in variations in scoring and which has been assessed in previous research. Second, variabilities in the phantom manufacturing processes have also been documented and may be compounded onto the viewer inconsistency. Ultimately the phantom image quality evaluation test for accreditation, as well as the phantom manufacture itself, involve human variabilities, the ramifications of which may not be acceptable in a national mammography program.

One approach to this problem is the use of computer-vision phantom image analysis to mitigate these effects. Generally this type of approach performs poorly, compared to humans, when interpreting complex scenes requiring higher-order human skills associated with memory and the visual cortex. However, the phantom image test objects are standard geometric shapes on a uniform background which, in comparison to actual patient mammograms, are simple and suggest that perhaps an automated, computer-vision system for evaluating the phantom images can match human acceptance levels for test objects in mammography phantom images.

As another approach, other researchers have demonstrated the success of statistical methods for comparing each facility's accreditation image against a standard image. In their study, relative contrast of the two largest microcalcification groups and three largest nodules was measured on MAP images of varying quality and a linear, least-squares relationship to a high-quality reference image was assumed. Though their quantitative image measurements did not include all of the test objects in the MAP phantom image, only three of the five nodules and two of the five microcalcification groups were utilized, the human

observer responses for these targets were well predicted by the quantitative, linear relationship with much less overall variance than the human observers.

SUMMARY OF THE INVENTION

The present invention addresses the problems described above by providing systems and methods for automating the scoring of phantom images. A Mammography Quality Control System according to the invention acquires digital images of test objects within a phantom. The MQCS processes the digital images to locate the test objects and, based on consistent objective criteria, evaluates the visibility of the objects. The classification is preferably performed using a baseline threshold established with actual human observations.

The MQCS may acquire digital images from a film or may acquire the digital images directly from a mammography unit. To acquire the digital images from the film, a light source illuminates the film and an imaging device, preferably a charge coupled device (CCD) acquires the digital images. These images are transferred to the MQCS for processing. The images of the test objects are preferably acquired directly with a digital imaging device thereby eliminating the need for any film or film processing. The mammography unit itself, for instance, may have an imaging plate for acquiring the digital images and these digital images are then transferred to the MQCS for analysis.

The MQCS performs signal processing to filter the digital images, locates the images of the test objects, and then evaluates the digital images. The MQCS preferably performs a Fast Fourier Transform (FFT) of the digital images, a convolution of the images with a mask, and then an inverse Fourier Transform. The result of this correlation is then passed to a classifier to determine whether images of the test objects are visible. The classifier uses a threshold established as a baseline of human observations. The MQCS preferably uses a two-hypothesis binary Bayesian classifier to assess the object's visibility.

Accordingly, it is an object of the present invention to provide systems and methods for scoring phantom images.

It is another object of the present invention to provide systems and methods for use in accrediting mammography unit.

It is still another object of the present invention to provide systems and methods that result in improved mammography images.

Other objects, features, and advantages of the present invention will become apparent with respect to the remainder of this document.

BRIEF DESCRIPTION OF THE DRAWINGS

The accompanying drawings, which are incorporated in and form a part of the specification, illustrate preferred embodiments of the present invention and, together with the description, serve to explain the principles of the invention. In the drawings:

Fig. 1 is a system for accrediting mammography units according to a first embodiment of the invention;

Fig. 2 is a diagram of an assembly to acquire digital images from film;

Fig. 3 is a more detailed block diagram of a Mammography Quality Control System (MQCS) shown in Fig. 1;

Fig. 4 is a schematic diagram of a mammographic accreditation phantom (MAP) showing the location and relative size of the features;

Fig. 5 is a spatial domain schematic depicting the correlation of f(x,y) and template g(x,y) at point (s,t);

Fig. 6(a) is an image of a simple object in spatial domain, Fig. 6(b) is a power spectrum of the simple object of Fig. 6(a), Fig. 6(c) is an image of a simple object rotated 45°, and Fig. 6(d) is a power spectrum of rotated simple object;

Figs. 7 and 8 are flow charts of a Mammography quality control program (MQCP) according to a preferred embodiment of the invention;

Figs. 9(a) to (e) are images of an original fiber image, of an appropriate binary mask, of an image power spectrum, of a mask power spectrum, and of a 2-D convolution of image of mask;

Figs. 10(a) to (e) are images of a speck group image, of an appropriate binary mask, of an image power spectrum, of a mask power spectrum, and of a 2-D convolution of image of mask;

Figs. 11(a) to (e) are images of an original mass image, of an appropriate binary mask, of an image power spectrum, of a mask power spectrum, and of a 2-D convolution of image of mask;

Fig. 12 is a diagram of an ideal centroid coordinates;

Fig. 13 is a plot of measured contrast versus percent visibility for fibers, specks and masses;

Fig. 14 is an image of Mammography Quality Control Program (MQCP) localization, film 5;

Fig. 15 is an image of Mammography Quality Control Program (MQCP) localization, film 2; and

Fig. 16 is a second embodiment of a system for accrediting mammography units.

DETAILED DESCRIPTION

Reference will now be made in detail to preferred embodiments of the invention, non-limiting examples of which are illustrated in the accompanying drawings.

I. PREFERRED SYSTEMS

With reference to Fig. 1, a mammography unit 12 acquires images of test objects embedded within a phantom 16 onto a film 14. Typically, this film 16 is evaluated by certified medical physicists who score the film 16 based on the perceived visibility of the objects and based on the existence of any image artifacts.

An arrangement 10 according to the invention, in contrast, employs a Mammography Quality Control System (MQCS) 20 for automatically performing an analysis on the film 14. The MQCS 20 eliminates the human errors in accrediting the mammography unit 12.

With reference to Fig. 2, the images on the film 16 are preferably captured and digitized with a charge coupled device (CCD) 36. The film 16 is placed within a Black Containment Box (BCB) 30 and the film 16 is illuminated with a light source 32. The BCB 30 preferably includes a collimator 34 for focusing the light from the source 32 and for reducing stray light onto the CCD 36. The images from the CCD 36 are supplied to an image capture unit 22 which digitizes the signals and passes the digitized signals onto a processing unit 24.

A more detailed diagram of the processing unit 24 is shown in Fig. 3. In the preferred embodiment, the processing unit 24 includes a Fast Fourier Transform (FFT) unit 41, a convolution unit 43, an inverse Fourier Transform unit 45, and a classifier 47. The digital images from the image capture unit 22 are input to the FFT unit 41 which converts the digital images of an image into the frequency space. The output of the FFT unit 41 is input to a convolution unit 43 which perform a convolution of the frequency domain signals with frequency domain signals of a mask. The shape of the mask, as will be described in more detail below, corresponds to the shape of the test object. The output of the convolution unit 43 is supplied to the inverse Fourier Transform unit 45 which converts the signals back to the time domain. From the output of the inverse Fourier Transform unit 45, a classifier 47 locates the images of the test objects and evaluates these images, such as by evaluating the contrast of the images. The MQCS 20 preferably also includes a report generator 49 for generating reports based on the data obtained with classifier 47. The operations of the FFT unit 41, convolution unit 43, inverse Fourier Transform unit 45, classifier 47, and report generator 49 is described in more detail below.

II. METHODS

A. Phantom

The phantom 16 may comprise any suitable phantom. As an example, the phantom 16 may be a commercially available breast phantom 16, preferably Model-156 Breast Phantom manufactured by Radiation Measurement Incorporated (RMI) of Middleton, Wisconsin, which meets MAP standards. With reference to Fig. 4, this standard mammographic phantom (SMP) 16 is constructed of a 10 cm by 10 cm by 4.5 cm thick acrylic block with a removable, tissue-equivalent wax insert 54 in one face (serial #312 156 type 4 phantom). The insert 54 is embedded with various sizes of nylon fibers 51 to simulate soft-tissue edges, aluminum oxide particles 52 to simulate microcalcifications, and water-density masses 53 to simulate tumors. These objects 51 to 53 represent common breast pathologies and are present in sizes that range from being easily visible to invisible in the phantom film image. The wax insert 54 is 0.4 cm thick and contains the fibers 51, microcalcification groups 52, and masses 53.

B. Mammographic Systems

The mammography unit 12 may comprise any mammography unit. For instance, the mammography unit 12 may be equipped with Molybdenum anodes and filtration: Suitable mammography units 12 include the General Electric Senograph 600T, Series HF Mammography Machine, manufactured by General Electric, in Moulineaus, France, and the LoRad M-II Mammography Machine, manufactured by LoRad Medical Systems, in Danbury, Connecticut. The General Electric machine 12 has a 0.3 mm focal spot size and a 65 cm source-to-image distance and the LoRad unit 12 has a 0.3 mm focal spot size and a fixed 50 cm source-to-image distance. All images are taken using standard 18 x 24 cm mammography film 16, such as the Min R E, manufactured by Kodak Company, of Rochester, New York, with a mammographic screen, such as the Kodak Min R,

and developed with the same undedicated darkroom film processor, such as the Kodak RP X-omat automatic processor.

In evaluating the performance of the MQCS 20, a set of eleven representative phantom films 16 are selected from fifty films 16 which were generated using these two machines 12 and various techniques. Main selection criteria used are the background optical density in the center of the film 16, which ranges from 0.61 to 2.50. Since a wide range of film densities are acceptable in the MAP, presumably because radiologists preferences span a range of background densities, films 16 are preferably selected which span the range of qualities expected from facilities participating in the ACR MAP with these techniques being listed below in Table 1. The units 12 are subject to routine quality control including the ACR MAP certification for both of the dedicated units 12.

Table 1

Film number	X-ray Unit	kVp	mAs	Optical density at film center
1.	LoRad	35	6	1.10
2.	LoRad	30	13	1.21
3.	LoRad	26	40	1.44
4.	LoRad	28	12	1.62
5.	SRM*	20	600	2.51
6.	GE	30	115	0.99**
7.	GE	30	82	0.66**
8.	GE	22	400	1.11
9.	GE	26	125	1.25
10.	GE	35	12	0.61
11.	GE	26	82	0.96
12.	GE	26	74	0.69

*SRM=Specimen Radiography Machine

**Includes 1.3 cm scattering media placed on top of phantom

A specimen radiography machine (SRM) such as the Faxitron series, 43807N X-Ray system, manufactured by Hewlett-Packard, of Pruneridge, California, is used to produce a reference phantom image. This machine is designed to operate for long exposures without tube damage and has a source-to-image distance of 56 cm. The same type of mammography film 16 is utilized and is also processed with an undedicated processor, such as the Kodak RP X-omat automatic processor. The remaining film 16 indicated in Table with No. 5 is obtained using a nonclinical technique with a 10-minute exposure on a typical specimen radiography unit with the phantom's wax insert 54 placed directly on the film 16, without an intensifying screen or cassette. A purpose for using a non-mammographic machine and technique for this film 16 is to maximize object visibility and produce a film 16 which approximates the upper bound of image quality. The eleven clinical technique films 16 all have less subject contrast and more blur than film number five.

C. Film Digitization

The smallest objects in the images are the last microcalcification group 52, at about 160 μm diameter. From Nyquist sampling frequency considerations, this indicates that the MQCS 20 should be capable of delivering an 80 μm spot size or smaller. Similarly, the range of optical densities represented spans nearly three optical density units, which indicates that the MQCS 20 preferably is capable of delivering into the thousands of unique gray values. The CCD 36 is preferably a cooled CCD, such as the Model 2300 manufactured by Photometries of Phoenix, Arizona, providing 2033 by 2045 each at 12-bits. The CCD camera 36 is installed in the Black Containment Box (BCB) 30 with the light source 32. The field-of-

view (FOV) of the camera 36 is adjusted to encompass the phantom image boundary. To minimize stray light, the light source 32 includes the collimator 34, which preferably comprises an opaque tray with a 10 cm square opening directly over the center of the light source 32. As an example of the light source 32, the light source 32 includes a bank of fluorescent cool-white light bulbs arranged along the edges of a two-foot square to yield an approximately flat, symmetrical light source in the center. The light source 32, opaque tray 34 and CCD camera 36 are all adjusted in their relative positions to yield maximum brightness values in the center of the brightest object in the phantom image while minimizing the exposure time and maintaining the FOV. The CCD chip 36 and the square opening in the collimator 34 are registered during digitization. This arrangement ensures the consistent alignment of images during digitization without regard to the degree of rotation of the phantom image relative to the edges of the film 16. The arrangement also allows the full spatial resolution of the CCD 36 to sample the 10 cm square which yielded approximately 50 μm/pixel in each direction.

The image capture unit 22 acquires and stores the images generated from the CCD camera 36. In one embodiment of the invention, the image capture unit 22 is a Macintosh IIfx computer which interfaces with the CCD camera 36 to acquire and store the images on an optical platter. The processing unit 24 comprises a UNIX workstation having a C compiler 24. The image capture unit 22 and processing unit 24, however, are not limited to this equipment. The image capture unit 22 and processing unit 24 comprise a single processing unit. The operations of the image capture unit 22 and processing unit 24 will be described in more detail below.

D. Model-Based Vision Computation

In analyzing SMP digitized film images, the processing unit 24 of the MQCS 20 preferably performs a constrained, two-dimensional, model-based recognition technique. The problem domain for the algorithm involves processing

two-dimensional digital images of specific test objects in the SMP images, localizing the objects and estimating their visibility according to experimentally measured observer data. The objects and approximate locations are defined *a priori*. The shapes include the rectangular-shaped fibers 51 slanted at +/- 45°, the circular-shaped microcalcifications 52 and the larger, disk-like simulated tumor masses 53. In order to accomplish the localization requirements, the MQCS 20 preferably does not drastically alter the spatial location of the shapes in the images. Constrained rotation of the fibers 51 (45°-rectangles) as well as translation of the fibers 51 and other shapes must be allowable. Given these initial constraints, the MQCS 20 preferably performs a template matching scheme for object localization.

1. *Frequency Domain Template Matching*

Figure 5 depicts a preferred template matching process in the spatial domain executed by the processing unit 24. The digitized images are 2033 pixels by 2045 pixels with a 10 cm^2 FOV by 12-bits/pixel due to the resolution requirements for sampling the 160 μm microcalcification group 52. This dictates a prohibitively large object image and template image for a spatial domain approach. Therefore, MQCS 20 utilizes a Fast-Fourier Transform (FFT) unit 41, which may alternatively perform decimation-in-time or a Cooley-Tukey algorithm. Two assumptions are that the array sizes are square and are evenly divisible by two and these conditions are met by the following digitization scheme. Equation 1 provides the mathematical definition of the continuous, two-dimensional Fourier transform, where:

$$F(u,v) = \int_{-\infty}^{+\infty}\int_{-\infty}^{+\infty} f(x,y)\exp[-j2\pi(ux+vy)]\,dx\,dy. \qquad \text{Equation 1}$$

The variables u and v are the associated frequency components for the x and y variables. The functions f(x,y) and F(u,v) are the Fourier transform pairs. The parameter $j = \sqrt{-1}$ is the standard imaginary number. The convolution theorem provides the means for using frequency domain correlation as an alternative to a

spatial domain approach. The theorem states that the spatial domain convolution, given by f(x,y)*g(x,y), is equivalent to the corresponding frequency domain relation F(u,v) · G(u,v) as shown in Equation 2.

$$f(x,y)*g(x,y) \Leftrightarrow F(u,v)\bullet G(u,v)$$
$$F(u,v)\bullet G(u,v) \Leftrightarrow f(x,y)*g(x,y)$$
$$f(r,\theta+\theta_o) \Leftrightarrow F(\omega,\varphi+\varphi_o) \qquad \text{Equation 2}$$

This is practically the process of centering the template image over the first pixel of the object image, multiplying the template's values by each value underneath it, replacing the original image pixels by the product and moving the template across the image in the spatial domain. In the frequency domain, this can be accomplished by the convolution unit 43 which simply multiplies the two Fourier-transformed functions and the inverse Fourier Transform unit 45 which performs an inverse transformation of the product. The continuous version of the convolution process is given by Equation 3.

$$f(x,y)*g(x,y)= \int_{-\infty}^{+\infty}\int_{-\infty}^{+\infty} f(\alpha,\beta)g(x-\alpha, y-\beta)\,d\alpha\,d\beta. \qquad \text{Equation 3}$$

Since an image is formed of quantified gray values, Equation 3 must be cast into discrete form. The two-dimensional, discrete Fourier transform is given by Equation 5, which follows from application of Equation 4 to Equation 1

$$f_e(x,y) = \begin{cases} f(x,y) & 0\le x\le A-1 \text{ and } 0\le y\le B-1 \\ 0 & A\le x\le M\text{-}1 \text{ and } B\le y\le N\text{-}1 \end{cases}$$

Equation 4

$$g_e(x,y) = \begin{cases} g(x,y) & 0\le x\le C-1 \text{ and } 0\le y\le D-1 \\ 0 & C\le x\le M\text{-}1 \text{ and } D\le y\le N\text{-}1 \end{cases}$$

$$F(u,v) = \frac{1}{N}\sum_{y=0}^{N-1}\sum_{x=0}^{N-1} f(x,y)\exp\left[\frac{-j2\pi(ux+vy)}{N}\right]$$

Equation 5

Equation 4 allows f(x,y) and g(x,y) to become discrete arrays with finite bounds of size A by B and C by D, respectively. Equation 6 follows from application of

Equation 4 to Equation 3. The values M and N are the assumed periodicity in the x and y directions, respectively

$$f_e(x,y)*g_e(x,y) = \frac{1}{N}\sum_{m=0}^{M-1}\sum_{n=0}^{N-1} f_e(m,n)\cdot g_e(x-m,y-n)$$

Equation 6

$$M \geq A+C-1$$

$$N \geq B+D-1$$

An issue of wrap-around error is of concern with the convolution process performed by the convolution unit 43. To completely avoid this error, the convolution unit 45 should preferably adjust images until the conditions for M and N in Equation 6 are met. It is sufficient to summarize this effect by stating that both the image f(x,y) and template g(x,y) need to be zero-padded out to the maximum positive or negative duration of the objects of interest. For instance, if an object of interest occupies the middle-half of an image, and the template is sized similarly, the convolution unit 43 must expand the template by adding zero values to perimeter locations until its array size is larger by one-half the dimension of the object. The convolution unit 43 must also increase the image in this fashion or, if it is already large enough to meet this requirement, the same corresponding locations must be either zero padded or ignored as they will be corrupted from wrap-around error. The process of zero-padding effectively selects a window of interest through which to view the image. This is unavoidable in practice since most images are of objects which are themselves finite in extent (i.e. non-zero mean). Unless the image is band-limited and periodic, all spatial frequencies cannot be completely recovered after forward and reverse Fourier transformations have taken place. The effect adds a small degree of blur to the inverse-transformed resultant image output by the inverse Fourier Transform unit 45. In the current context, this loss of very high-frequency information is negligible since the Fourier results are used for relative correlation coefficient estimation and this error does not affect the original image values or the contrast calculation.

Since the FFT unit 41 performs a symmetric linear operation, arbitrary translation and rotation of the test images is maintained throughout Fourier space processing. This is demonstrated by Figure 6 where the power spectrum rotates along with the object, assuring that the FFT will not alter the original translation and rotation of the image information. The power spectrum display represented in Equation 7 below allows visualization of the Fourier frequency domain information.

$$P(u,v) = R^2(u,v) + I^2(u,v) \qquad \text{Equation 7}$$

The terms R(u,v) and I(u,v) are the real and imaginary components of the transformed function, F(u,v). This is also evident in the polar coordinate representation of the convolution theorem statement provided by the last line of Equation 2.

2. *Object Localization Algorithm*

The operation of the MQCS 20, which includes the functions performed by the FFT unit 41, convolution unit 43, inverse Fourier Transform unit 45, classifier 47, and report generator 49, are described below with reference to a Mammography Quality Control Process (MQCP) 80 according to a preferred embodiment of the invention. Figure 7 and Figure 8 depict an example of the MQCP 80. An assumption made in MQCP 80 is that the digitized input images are cropped or optimally digitized at the apparent edge of the wax insert 54. This assumption is readily met in practice by the CCD device 36 and the BCB 30. If the film 16 is translated during digitization, the result will become evident in the displacement report but this will not add error to the localization process unless the film 16 is shifted more than about 1 cm or more. The rotation and translation independent nature of the MQCS 20 provides this immunity. The 1 cm limit is due to the constraints of the phantom manufacturer whereby any displacement error of more than a few millimeters is sufficient for rejection. Thus, these constraints are utilized in MQCP 80 to limit the search areas.

The Fourier-domain template matching approach used at the start of the MQCP 80 through the Fourier Transform unit 41, provides only a partial measure of object localization. Following Figure 7, the MQCS 20: (1) reads the image and its dimensions and scale; (2) extracts the first sub-image and performs its FFT with FFT unit 41; (3) either reads a pre-computed mask-FFT (shaded lines in Figure 7) for the particular shape or generates a zero-centered, binary mask for the shape and performs the FFT; (4) the object FFT and the mask FFT are then multiplied, element-by-element, to perform the convolution with convolution unit 43; (5) the inverse-FFT is performed by the inverse Fourier Transform unit 45 on the product image; (6) the resultant image is a matrix of correlation coefficient values indicating the degree of correlation the template exhibited for the value's location in the original image. The MQCP 80 is shown with corresponding images in Figs. 9 to 11 for the three shapes. For the second portion of the MQCP 80, shown in Figure 8, the correlation surface resulting from part 1 is searched for maxima in the search ranges determined *a priori* and these locations are stored. Typical maxima are indicated in Figs. 9 to 11. Since one objective for fibers 51 is to measure the amount of rotation, the ideal angle for a particular fiber 51 was used to create the mask and minor angular differences between the mask and the actual grayscale image do not appreciably affect measurement of the underlying fiber angular placement error. The same argument holds for displacement error of the other shapes 52 and 53. This effect should be apparent in Figure 10, where only a portion of the speck group 52 is used as an input image and the approach localizes the specks 52 in a correctly registered, correlation surface image. This is true as long as displacement is no more than the manufacturer specified 1 cm in any direction for all three shapes, including individual specks 52.

The fiber correlation surface, shown in Figure 9, is essentially a ridge of high values which are somewhat noisy, depending upon the noise and artifact levels in the original image. Multi-element, uni-directional derivative filters are used that demonstrate the peak values of fiber correlation or maximum ridge as

referred to in Figure 9. The results from the filter testing are used to select the optimal filter size for MQCS's 20 localization of fiber peak values. The peak values of fiber correlation can deviate from a straight line depending on the image noise and the amount of dislocation of the fiber 51 relative to the sub-image lateral boundaries. The latter effect is due to the frequency-domain errors associated with the FFT convolution approach as discussed previously. To avoid these effects, the MQCS 20 considers the peak values only around a 1 cm square vicinity of the ideal, *a priori* fiber location. The image noise may still cause a discontinuity in the ridge values which fall inside this spatial constraint. This effect is handled by iteratively selecting portions of the ridge until a section, as long as the particular fiber 51 is wide, gives angles from a least-squares fit to within 10° of the *a priori* 45°. If the constraint is not met after ten iterations, MQCP 80 will stop searching and default to the *a priori* location as the centroid coordinates. Equation 8 mathematically describes the least-squares fit used by the MQCS 20 in the MQCP 80. The angle was taken as the inverse tangent of the slope from the least-squares fit where: xi = peak location i, x-coordinate; yi = peak location i, y-coordinate; n = total number of peak values.

$$angle = \tan^{-1}\left[\frac{\left(\sum_{i=1}^{n} x_i y_i - \left(\sum_{i=1}^{n} x_i \sum_{i=1}^{n} y_i\right)\right)}{\sum_{i=1}^{n} x_i - \frac{\left(\sum_{i=1}^{n} x_i\right)^2}{n}}\right]$$

Equation 8

The peak values should include the numerically largest value of correlation in the image. However, a minor discrepancy could arise from application of the derivative filter used to find the peak values. If this occurs, the final centroid coordinates for a fiber 51 are taken to be the x-coordinate from the maximum

correlation location and the y-coordinate is taken as the peak value corresponding to the x-coordinate. Since the specks 52 and masses 53 are rotationally symmetric, there is no angular error component. The ideal locations for all 16 objects are schematically depicted in Figure 12. These locations are measured from the edges of the image thus it is assumed that the input images are cropped at the wax edges as previously discussed. The centroid coordinates are selected which are within 1 cm of the ideal locations shown in Figure 12 and the maximum of the correlation surface in the same search area. The speck groups 52 are arranged in the corners and center of a regular pentagon. The ideal location of the center of the speck group 52 is assumed to coincide with the location shown in Figure 12 where specks 52 occur. The ideal locations of the remaining specks 52 in a given group are measured relative to the coordinates of a pentagon centered about the coordinates shown in Figure 12. The displacement errors are measured by the standard distance formula applied to the MQCP 80 located centroid coordinates and the ideal coordinates for a particular shape.

3. *Object Visibility*

Once the location of a particular shape is estimated, the contrast of the shape is determined. The classifier 47 in the MQCS 20 calculates the contrast according to Equation 9 shown below, where: S = signal, average gray value of located object; B = background, average value of area surrounding located object; dark = dark current of camera system, if applicable.

$$C = \frac{S - dark}{S + B - dark} \qquad \text{Equation 9}$$

The background area dimensions are selected which encompass enough background area to provide a stable average gray-value for the region. The MQCS 20 utilizes a comparable area of surround, or greater, on each dimension of the object. The MQCS 20 indicates the areas used as signal and background by marking the closest outside pixel black at the border of each region of interest.

This computer graphics feature allows the MQCP 80 localization results to be quickly analyzed for accuracy. Samples of this process are provided in the Examples section below.

Final classification of the localized objects is performed by the two-hypothesis binary Bayesian classifier 47. The classification variable is threshold contrast, Ct, and the decision for visibility is assumed to be at 50% visibility. Implementation of this classifier 47 is accomplished by comparison of a particular shape's contrast with the threshold value for that shape and establishing visibility if it is greater than the threshold and non-visibility if it is less than the threshold. The observer data were taken from previously presented measurements. The Examples section below contains the determination of Ct for the three shapes used in MQCP 80.

Testing of MQCP 80 against humans for ACR passing rates was performed for six images which had a moderate observer response rate. That is about half as many passed the images as failed them. Human observers in the present work did not include scoring of artifacts or partial object visibility. The moderate response rate for these films 16 assured that a human threshold was encountered in each shape category, because a portion of the human observer population had to fail the images for the response rate to be moderate. The images used were digitized from film numbers: 1, 2, 3, 5, 6 and 10 of those listed in Table 1. The same images were also used to train the binary classifier 47 by establishing the threshold contrasts for each shape. While using the same images to both establish a threshold and test the threshold could lead to bias in the classifier 47, the objective of this work is to demonstrate that automated processing is feasible. A universally applicable threshold or other decision metric derived from actual ACR cases may be implemented.

For displacement error testing, three SMP wax inserts 54 were used from a selection of rejected SMPs from the phantom vendor. These inserts 54 were specifically rejected because of their displacement errors. Each image represents a

rejection based upon one shape. The known errors consist of: film 1, the fifth fiber 51 is significantly rotated past 45°; film 2, the third speck group 52 has a severely displaced speck; and film 3, the last mass 53 is severely displaced. The errors were quantified by physically estimating displacement or rotational deviation from estimated ideal conditions. SMP film images were digitized with CCD camera 36 and the pixels manually counted. The ideal conditions were estimates used to demonstrate that MQCS 20 could quantify errors. Comparison of results from using the MQCP 80 and the measured errors are provided in the results in Table 2 shown below.

Table 2

Film Number	Error	Angle (°)	MQCP Angle (°)	Distance (cm)	MQCP distance (cm)
1.	fiber angle	72	69.7	n/a	n/a
2.	speck	n/a	n/a	1.64	1.78
3.	mass	n/a	n/a	1.93	2.04

After the MQCS 20 has estimated location, errors, contrast and visibility for all shapes, the processing unit 24 generates final output reports at step 120 through the report generator 49, summarizing this information. Sample output results from MQCP 80 for a test image are provided in the results in Tables 3 and 4 shown below. The results include displacement errors and rotation errors for fibers, displacement errors for speck groups, and masses, contrast information for the above as well as a final ACR passing decision based on the object visibility scores.

Table 3

Contrast and Visibility Report:

Fibers	Contrast (Min. 1.010)	Visible
1	1.093	Yes
2	1.079	Yes
3	1.069	Yes
4	1.060	Yes
5	1.034	Yes
6	1.031	Yes

Number fibers visible: 6 (ACR Requirement: 4)

Speck	Contrast (Min. 1.156)						
Groups	1	2	3	4	5	6	Visible
1	1.276	1.329	1.342	1.327	1.318	1.309	Yes
2	1.570	1.578	1.544	1.534	1.323	1.602	Yes
3	1.502	1.546	1.578	1.571	1.610	1.611	Yes
4	1.338	1.332	1.441	1.360	1.453	1.375	Yes
5	1.130	1.132	1.101	1.107	1.067	1.089	No

Number speck groups visible: 4 (ACR Requirement: 3)

Masses	Contrast (Min. 1.016)	Visible
1	1.229	Yes
2	1.121	Yes
3	1.098	Yes
4	1.057	Yes
5	1.023	Yes

Number of masses visible: 5 (ACR Requirement: 3)

Displacement report (mm from ideal)

Fiber #	Right (+) Left(-)	Up(+) Down(-)	Centroid Distance	Rotation Angle (degrees)
1	-1.498	-0.005	1.498	45.324
2	6.840	0.277	6.846	-46.685
3	11.094	-0.756	11.120	45.987
4	20.277	-1.366	20.323	-43.953
5	-1.545	-10.643	10.755	44.678

6	4.305	-5.432	6.931	-45.000		
Speck	Centroid Distance					
Group #	1	2	3	4	5	6
1	13.507	13.943	14.962	15.441	13.515	11.622
2	19.902	19.325	21.255	21.453	19.265	17.888
3	12.599	10.662	12.337	15.005	14.330	12.297
4	13.405	12.598	14.697	15.892	14.956	12.979
5	18.485	16.799	18.746	15.410	15.756	15.765

Mass #	Right (+) Left(-)	Up(+) Down(-)	Centroid Distance
1	18.587	-12.174	22.219
2	-0.136	-19.103	19.104
3	0.418	-19.291	20.331
4	12.784	-19.291	23.143
5	18.164	-17.930	25.523

Table 4

Contrast and Visibility Report:

Fibers	Contrast (Min. 1.010)	Visible
1	1.019	Yes
2	1.014	Yes
3	1.009	No
4	1.002	No
5	1.003	No
6	1.005	No

Number fibers visible: 2 (ACR Requirement: 4)

Speck	Contrast (Min. 1.156)						
Groups	1	2	3	4	5	6	Visible
1	1.123	1.201	1.111	1.076	1.167	1.195	No
2	1.195	1.193	1.122	1.162	1.083	1.165	Yes
3	1.166	1.234	1.236	1.229	1.245	1.178	Yes

4	1.101	1.123	1.131	1.169	1.138	1.154	No
5	1.115	1.085	1.142	1.099	1.115	1.074	No

Number speck groups visible: 2 (ACR Requirement: 3)

Masses	Contrast (Min. 1.016)	Visible
1	1.061	Yes
2	1.023	Yes
3	1.021	Yes
4	1.003	No
5	1.007	No

Number of masses visible: 3 (ACR Requirement: 3)

Displacement report (mm from ideal)

Displacement (mm from ideal)

Fiber #	Right (+) Left(-)	Up(+) Down(-)	Centroid Distance	Rotation Angle (degrees)
1	2.493	6.991	7.422	45.567
2	6.418	0.230	6.422	-45.749
3	8.700	0.324	8.706	45.134
4	11.451	6.991	13.416	-46.987
5	-3.469	0.812	3.563	46.005
6	8.296	0.390	8.305	-46.003

Speck	Centroid Distance					
Group #	1	2	3	4	5	6
1	10.957	11.0691	12.404	12.802	10.924	9.131
2	17.200	16.713	18.468	18.612	16.860	15.646
3	10.876	9.066	10.413	13.049	12.710	10.865
4	12.480	10.183	12.161	13.514	12.717	10.675
5	14.778	13.563	20.137	15.850	15.165	13.306

Mass #	Right (+) Left(-)	Up(+) Down(-)	Centroid Distance
1	17.742	-9.732	20.236
2	-2.155	-16.991	17.127
3	4.681	-17.460	18.077
4	9.920	-11.310	15.044

5	21.028	-12.577	24.503

II. EXAMPLES

A. Automated Localization Performance

Table 2 contains the comparison between MQCP 80 and measured distances for displacement errors as well as angle error for the three films 16 which failed the phantom vendor's quality control requirements. The distances given are centroid displacement distances, measured relative to Figure 12. Both the angle errors and the distance errors indicate that the MQCS 20 is capable of tracking displacements and angular error relative to any arbitrary reference frame. This is also evident from the results shown in Figure 14 for film number 5. The observer passing response for this film was unanimous at 100%. These results are indicative of the localization performance expected from MQCS 20 when a very good quality image is provided and high-resolution digitization used. For film number 2, the MQCP 80 localization performance is shown in Figure 15. These results are indicative of a film 16 which is only marginally meeting the ACR passing rate criterion. This film averaged less than 50% passing rate from all of three groups of thirty observers each. The image is noisy and all of the objects are not necessarily visible to the human eye.

B. MQCS Performance

The results from training MQCP's binary decision classifier 47 are shown in Figure 13. The low spatial frequency objects, fibers 51 and masses 53, exhibit very similar contrast visibility and are distinct from the response for high spatial frequency objects, specks 52, for the observers tested. These results are in agreement with similar results presented previously. The threshold contrast values corresponding to the decision probability of 50% visibility were: fibers 1.010;

specks 1.156; and masses 1.016. These values were utilized in MQCP to test for visibility of located objects.

The results from testing MQCP 80 with six test images and comparing them to human judgments are shown below in Table 5. The contrast, visibility and displacement error results are summarized in Tables 3 and 4 for the two images shown in Figs 14 and 15, respectively. Localization graphics for these images indicate the areas used for signal and background in the contrast calculation. The MQCS 20 gave the same object scores as humans for Film 5, as shown in Fig. 14. This was evidence of the ability of the MQCS 20 to correctly operate on extremely good images. Film 2 gave conflicting results between MQCS 20 and the trained diagnostic physicists. The reason film 2 failed was due to the fact that only half of the fourth fiber 51 is actually visible. The observers were instructed to make a judgment between visible or non-visible, though 40% of the trained observers commented that the fiber 51 was half-visible while viewing this film 16. Thus the contrast is lowered by an appreciable amount causing it to drop below the threshold. In this instance, the binary classifier 47 still comes very close to reaching the same decision as humans (off by 10%). The specks 52 and masses 53 for film 2 registered passing scores with the MQCS 20 as they did with humans. A more complex classifier, such as a multi-hypothesis decision rule may provide closer results in these cases. The MQCS 20 passed or failed the remaining films the same as the human observers.

Table 5

Film Number	MQCP	Trained-Physicist ACR Passing Rate
1	Fail (<50% probability)	40% passed
2	Fail (<50% probability)	60% passed
3	Pass (<50% probability)	100% passed
5	Pass (<50% probability)	100% passed

6	Fail (<50% probability)	20% passed
10	Fail (<50% probability)	40% passed

III. DISCUSSION

Since current SMP phantom designs do not provide an absolute reference frame such as fiducial markers, the MQCS 20 locates the test objects autonomously. To help with this, a digitization mask is used which crops the film image at the apparent edge of the wax insert. At this point, the images are positioned so that the shapes are in a known order. Having properly digitized the images, the image processing is performed in two stages: object localization and object visibility. First, object localization is crucial since no attempt to model visual responses can work without first finding gray values which have a high probability of being related to the correct objects. Thus, low-level processing utilizing Fourier domain template matching is employed to provide a registered map of correlation coefficients. Intermediate-level processing utilizes derivative filters operating on the correlation coefficient map to find local maxima. The MQCP 80 performs at least as well as humans and without human variability and actually performs better since the MQCS 20 has access to much more information than the human eye can process. The final stage of processing is the high-level classification which is modeled by a Bayesian classifier 47 using threshold contrast as measured from the target observer group. Threshold contrast has been identified as a useful predictor variable for estimating human visibility. The performance by MQCP 80, coupled with a cooled CCD 36 2033 by 2045 by 12-bit camera digitizer, is in good agreement, overall with specially-trained human observers.

V. VARIATION

A second embodiment of the invention is shown in Fig. 16. According to this embodiment, rather than using film 16 to acquire images of a phantom 16, a mammography unit 12' uses an imaging plate 30. The imaging plate 30 comprises any suitable digital imaging plate, such as a solid state imaging plate. The digital images are then supplied directly to the MQCS 20'.

The mammography unit 12' improves the quality of mammography images by eliminating the entire film 16 and need for film processing. The film 16 and processing of film has a high potential of introducing artifacts to the image. These artifacts, for example, may be introduced by poor handling techniques that scratch or otherwise mark the surface of the film 16.

Although artifacts associated with the film 16 or film processing are reduced if not eliminated through the use of the mammography unit 12', the reliance on the imaging plate 30 may introduce other types of artifacts onto an image. For instance, a phenomenon called "blooming" occurs when the charge in one pixel area overflow into another pixel area. The overflow in charges from one pixel to another pixel area produces erroneous bright spots. As another example, the imaging plate 30 may have a dark current or dark signal. When a portion of an image should be entirely blank, spurious signals detected by the imaging plate 30 might show up on the image along the gray scale, producing erroneous results.

The need for systems and methods for performing automated analysis of phantom images therefore still exists even if the film 16 is not used. The MQCS 20' differs from the MQCS 20 in that the MQCS 20' does not need the BCB 30, CCD camera 36, light source 32, and collimator 34 to acquire the digital images. Instead, the MQCS 20' preferably interfaces directly with the imaging plate 30 within the mammography unit 12.' Alternatively, the MQCS 20' may connect to an interface in the mammography unit 12'. For instance, direct imaging plate technology (amorphous silicon) may be used for breast imaging. With direct imaging plate technology, film images 16 will no longer be available to send into the FDA(HHS) for compliance with the MQSA and instead the FDA can accept

purely digital versions of the MQSA breast phantom images. By obtaining the digital signals directly from the imaging plate 30, the MQCS 20' can more accurately detect phantoms, artifacts, beam quality, dosage, spatial resolution and contrast and would not be prone to any errors associated with film processing or film digitizing.

As another alternative, the MQCS 20' may obtain the digital images from a mammography unit 12' which is located at a remote location through an intermediate interface 140. A great advantage of eliminating the film 16 is that the images of phantoms can be easily transmitted to the MQCS 20'. The interface 140, for instance, may be the Public Switched Telephone Network (PSTN), the Internet, a wireless link, a satellite link, a dedicated data link, or any other type of communication link. The interface 140 may also include an intermediary, such as a computer or storage area.

The entire accreditation process can thus be altered with the MQCS 20'. Rather than forwarding film 16 from a mammography unit 12 to the FDA or state entity, which then relies upon medical physicists to score, the images of the phantoms can be transmitted electronically to the MQCS 20'. The mammography units 12' may send its data directly to the MQCS 20' or, alternatively, to the FDA or state entity involved in analyzing the images. The MQCS 20' may receive the digital images from the FDA or state entity or it may be resident within the FDA or state entity. Moreover, the invention is not limited to mammography accrediting in the U.S. but may be applied in other countries, either for accrediting purposes or for other quality control reasons.

The forgoing description of the preferred embodiments of the invention has been presented only for the purpose of illustration and description and is not intended to be exhaustive or to limit the invention to the precise forms disclosed. Many modifications and variations are possible in light of the above teaching.

For example the invention has been described with reference to systems and methods for accrediting mammography units. The invention, however, may be

used for other purposes, such as in a self-diagnostic test performed by a mammography unit. The mammography unit can periodically perform a self-diagnostic test which involves imaging a phantom and analyzing the resultant images. From these tests, the mammography unit can be altered to optimize its performance.

Additionally, the MQCS may be used in quality control of the phantoms themselves. Phantoms presently differ from one manufacturer to the next and even may vary within a single manufacturer. One manufacturer, for instance, may use different materials in constructing a phantom than another manufacturer and may slightly alter the placement, size, or even shape of a test object. Further, even within a single manufacturer, phantoms are often hand made and, accordingly, the shape, material, size, and placement of a test object may vary from one phantom to the next phantom. These variations in the phantoms themselves cause variations in the images of the test objects. To allow for the more uniform manufacture of phantoms, the MQCS may be used in quality control, such as by identifying those phantoms that deviate beyond established quality control guidelines. These guidelines may be established internally by the manufacturer or may even be mandated by a government.

The embodiments were chosen and described in order to explain the principles of the invention and their practical application so as to enable others skilled in the art to utilize the invention and various embodiments and with various modifications as are suited to the particular use contemplated.

We claim

1. A system for use with a mammography unit that generates a digital image of a phantom containing test objects, comprising:

a Fourier transform unit for receiving the digital image of the phantom and for converting the digital image from a time domain into a frequency domain and for outputting frequency domain image signals;

a convolution unit for receiving the frequency domain image signals and for convoluting these signals with frequency domain mask signals, the convolution unit generating convolution output signals;

an inverse Fourier transform unit for converting the convolution output signals from the frequency domain to the time domain and for outputting processed time domain image signals; and

a classifier for receiving the processed time domain image signals and for evaluating a visibility of the test objects using objective criteria.

2. The system as set forth in claim 1, further comprising a report generator for generating a report on results of the classifier.

3. The. system as set forth in claim 1, wherein the Fourier transform unit receives the digital image directly from the mammography unit.

4. The system as set forth in claim 1, wherein the Fourier transform unit receives the digital image through an interface.

5. The system as set forth in claim 1, wherein the Fourier transform unit receives the digital image from a remote location.

6. The system as set forth in claim 5, wherein the Fourier transform unit receives the digital image over a network.

7. The system as set forth in claim 6, wherein the network is the Internet.

8. The system as set forth in claim 6, wherein the network is the Public Switched Telephone Network.

9. The system as set forth in claim 4, wherein the interface comprises a storage area.

10. The system as set forth in claim 4, wherein the interface comprises a computer.

11. A method for analyzing a digital image of a phantom containing test objects for use with a mammography unit that generates the digital image, comprising the steps of:

receiving the digital image of the phantom and performing a Fourier transform and outputting a set of frequency domain image signals;

performing a convolution of the set of frequency domain image signals with a set of frequency domain mask signals to generate convolution output signals;

performing an inverse Fourier transform of the convolution output signals and outputting processed time domain image signals; and

receiving the processed time domain image signals and evaluating a visibility of the test objects using objective criteria.

12. The method as set forth in claim 11, wherein the step of receiving the digital image comprises a step of receiving the digital image directly from the mammography unit.

13. The method as set forth in claim 11, wherein the step of receiving the digital image comprises a step of receiving the digital image from the mammography unit through an intermediate interface.

14. The method as set forth in claim 11, wherein the step of receiving the digital image comprises a step of receiving the digital image through the Internet.

15. The method as set forth in claim 11, wherein the step of receiving the digital image comprises a step of receiving the digital image through the Public Switched Telephone Network.

16. The method as set forth in claim 11, wherein the step of receiving the digital image comprises a step of receiving the digital image from a storage area.

17. The method as set forth in claim 11, wherein the step of receiving the digital image comprises a step of receiving the digital image from a remote location.

18. The method as set forth in claim 11, wherein the step of receiving the digital image comprises a step of receiving the digital image from a computer.

19. The method as set forth in claim 11, further comprising a step of generating a report based on results of the step of evaluating.

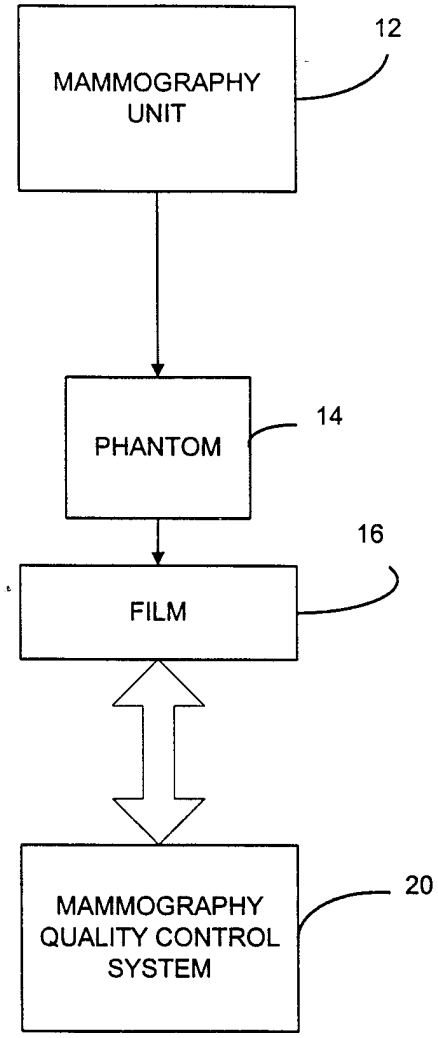
MAMMOGRAPHY UNIT
12
PHANTOM
14
FILM
16
MAMMOGRAPHY QUALITY CONTROL SYSTEM
20

FIG. 1

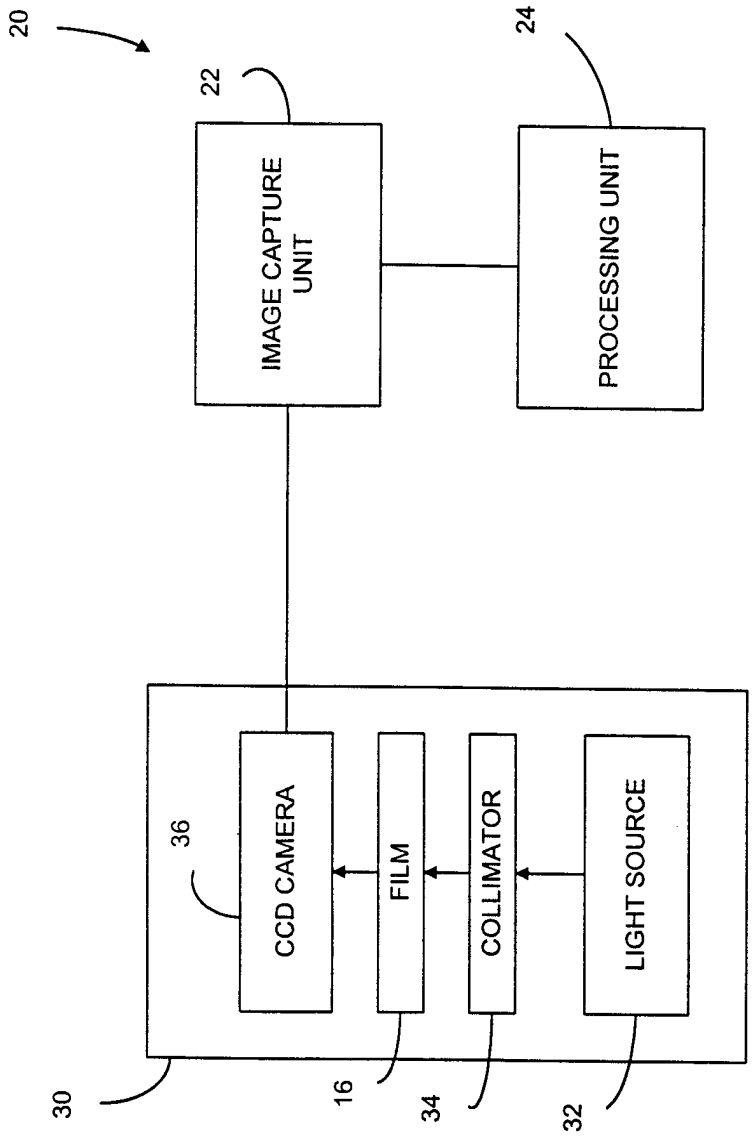
20
22
IMAGE CAPTURE UNIT
24
PROCESSING UNIT
36
CCD CAMERA
FILM
COLLIMATOR
LIGHT SOURCE
30
16
34
32

FIG. 2

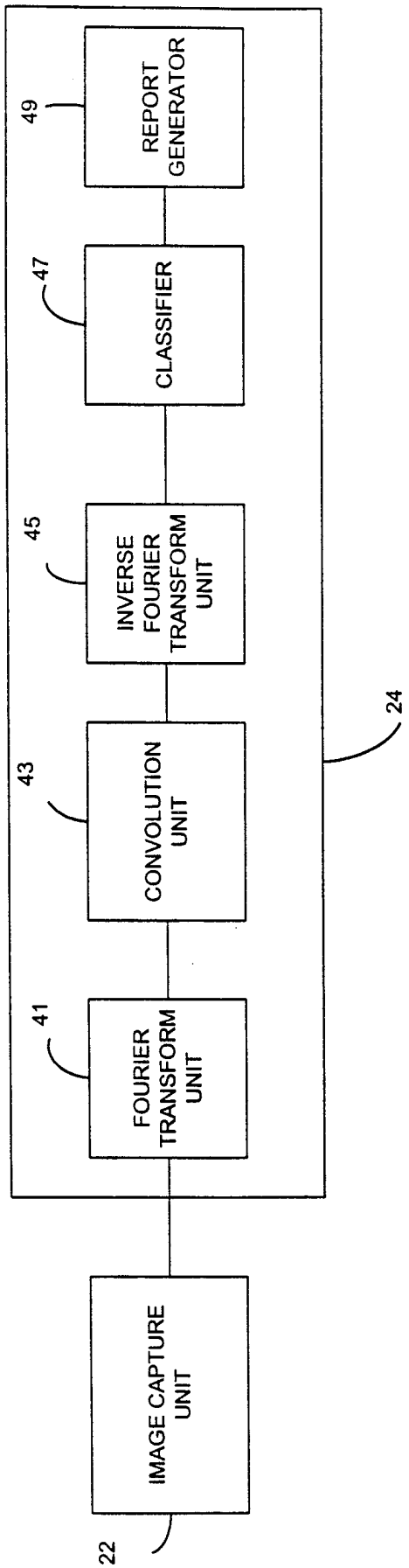
IMAGE CAPTURE UNIT
22
FOURIER TRANSFORM UNIT
41
CONVOLUTION UNIT
43
INVERSE FOURIER TRANSFORM UNIT
45
CLASSIFIER
47
REPORT GENERATOR
49
24

FIG. 3

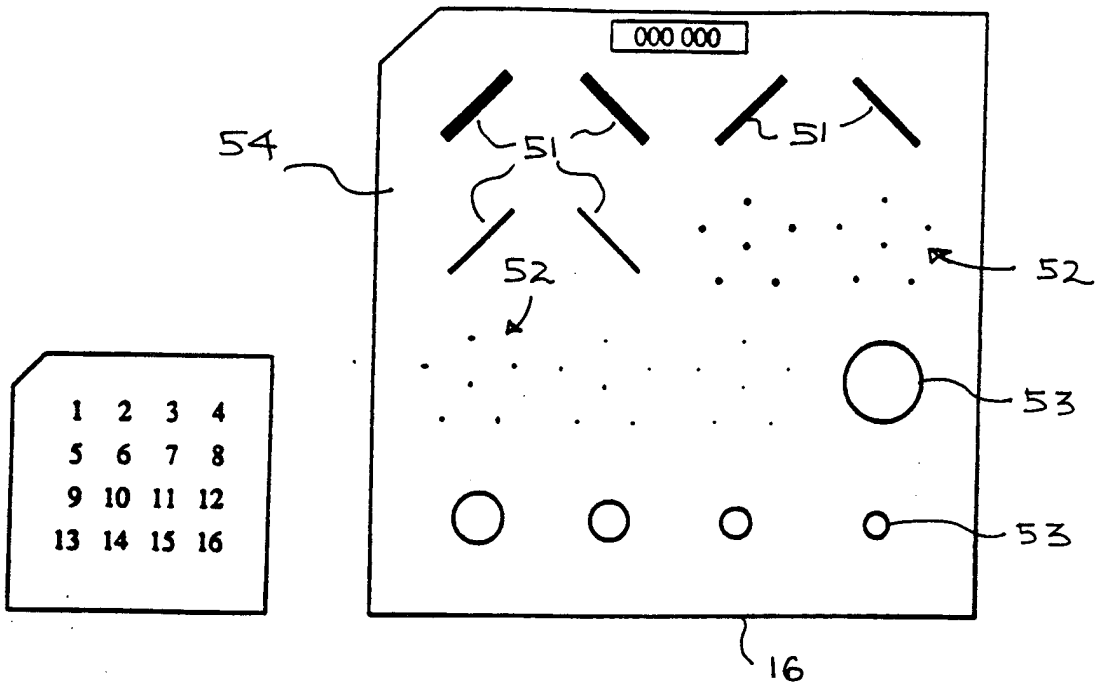

Object Number	Dimensions	Region Materials
1	1.56 mm (thickness)	nylon fiber
2	1.12 mm (thickness)	nylon fiber
3	0.89 mm (thickness)	nylon fiber
4	0.75 mm (thickness)	nylon fiber
5	0.54 mm (thickness)	nylon fiber
6	0.40 mm (thickness)	nylon fiber
7	0.54 mm (diameter)	Al_2O_3 speck group
8	0.40 mm (diameter)	Al_2O_3 speck group
9	0.32 mm (diameter)	Al_2O_3 speck group
10	0.24 mm (diameter)	Al_2O_3 speck group
11	0.16 mm (diameter)	Al_2O_3 speck group
12	1.00 mm (diameter)	mass
13	0.80 mm (diameter)	mass
14	0.70 mm (diameter)	mass
15	0.50 mm (diameter)	mass
16	0.40 mm (diameter)	mass

FIG. 4

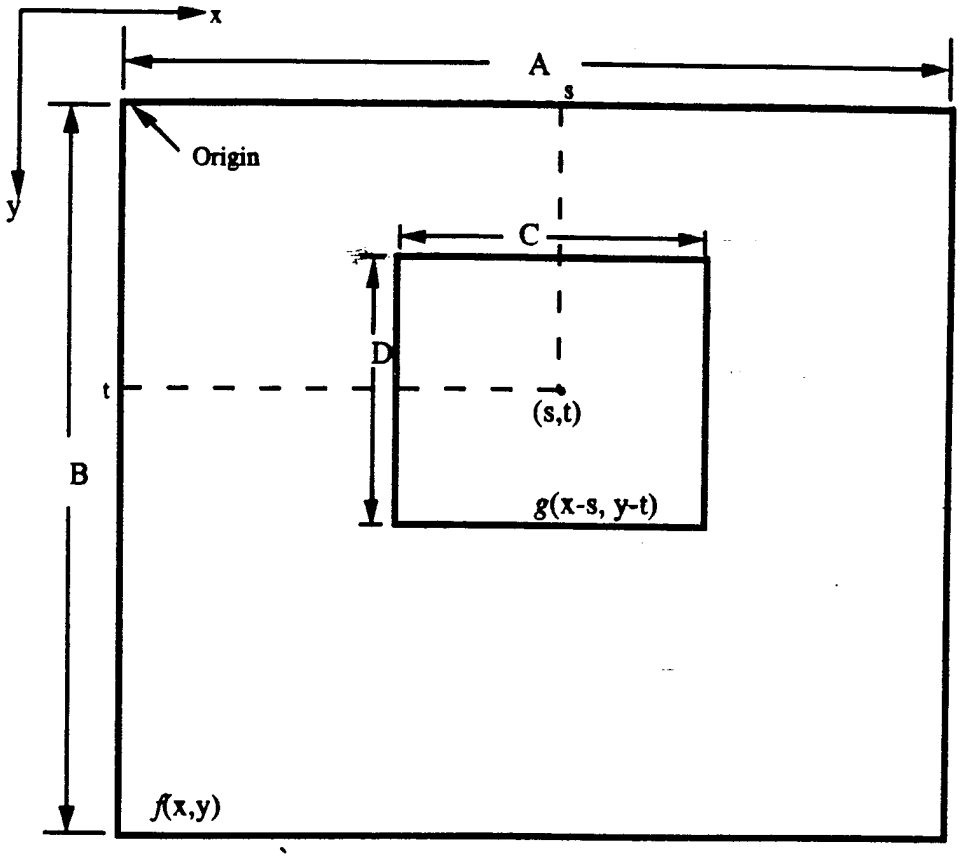

FIG. 5

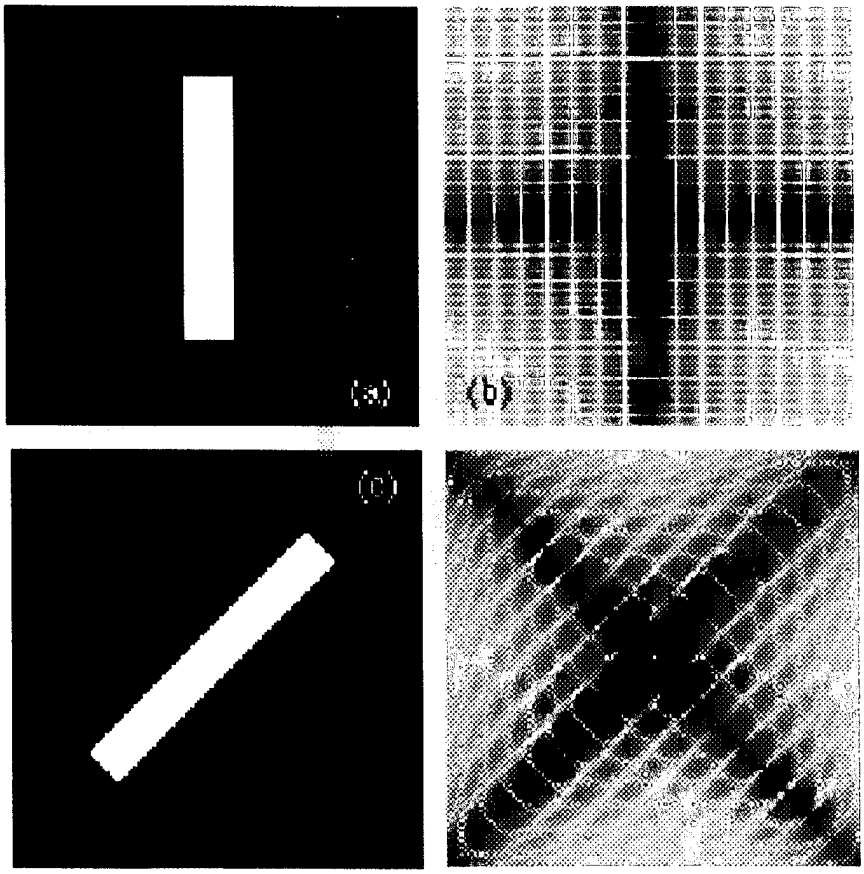

FIG. 6

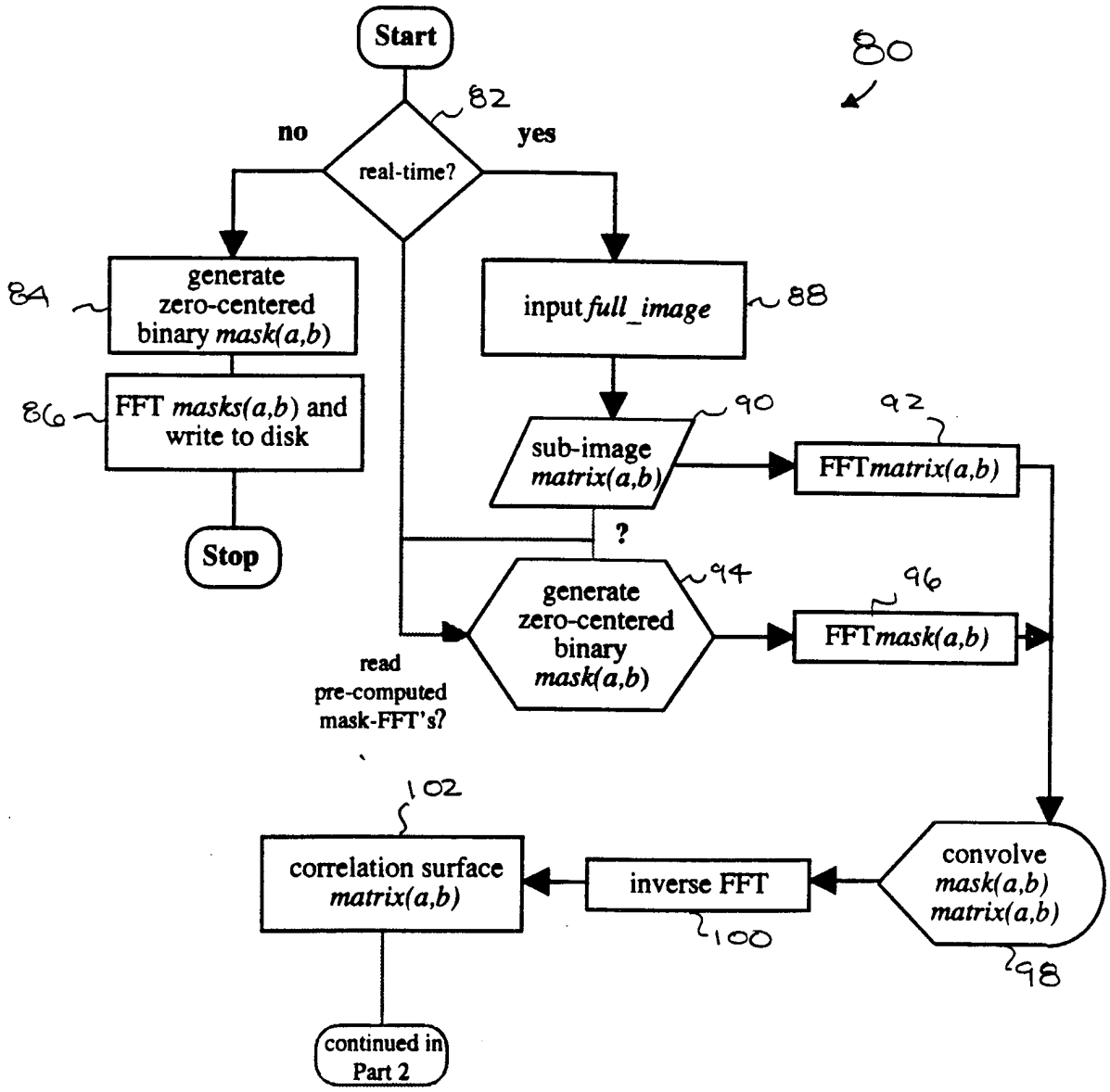
Start
80
82
no
yes
real-time?
84
generate zero-centered binary mask(a,b)
86
FFT masks(a,b) and write to disk
Stop
input full_image
88
90
sub-image matrix(a,b)
92
FFTmatrix(a,b)
?
94
generate zero-centered binary mask(a,b)
96
FFTmask(a,b)
read pre-computed mask-FFT's?
102
correlation surface matrix(a,b)
inverse FFT
100
convolve mask(a,b) matrix(a,b)
98
continued in Part 2

FIG. 7

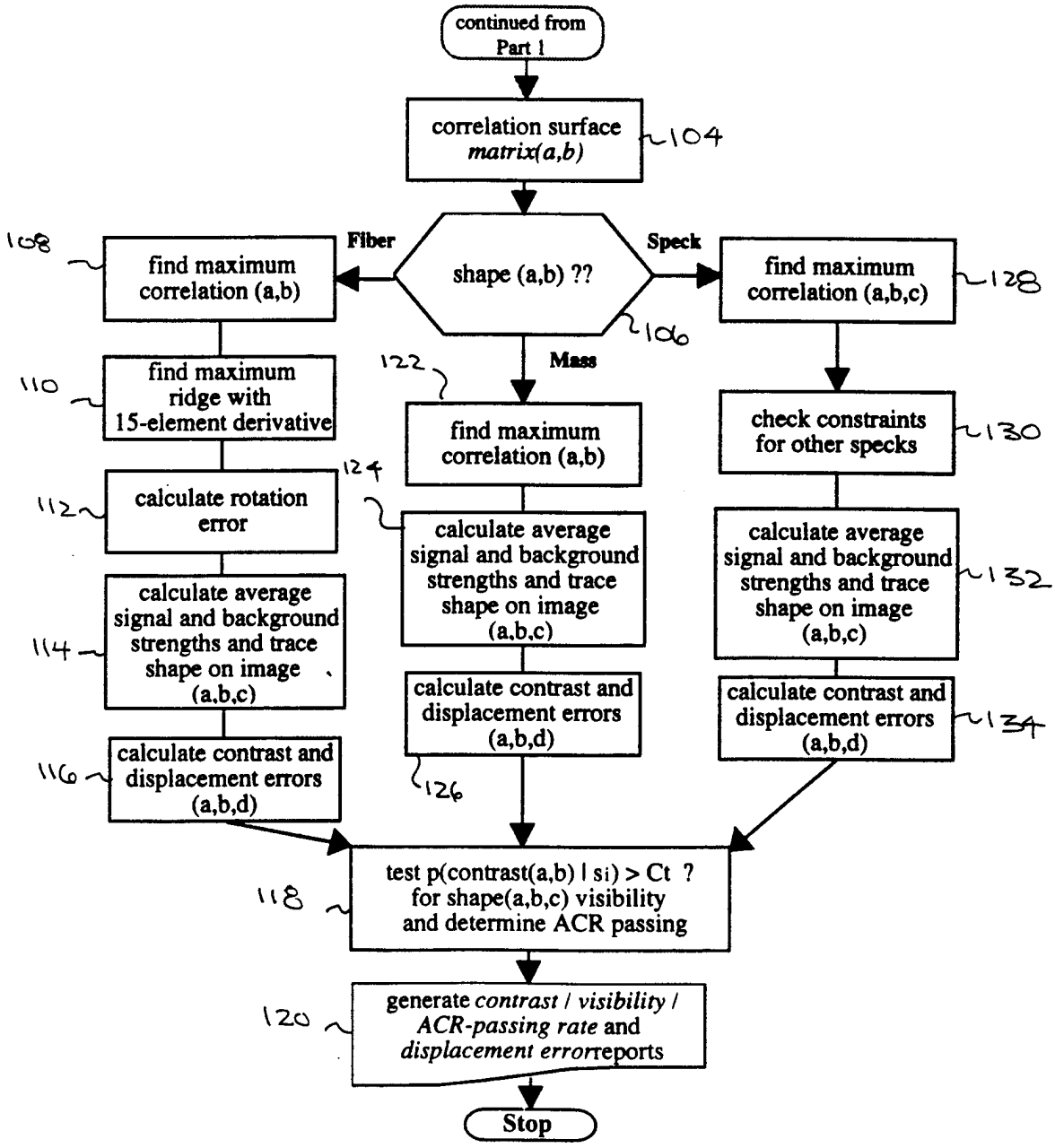
continued from Part 1
correlation surface matrix(a,b)
104
shape (a,b) ??
106
Fiber
Speck
Mass
108
find maximum correlation (a,b)
110
find maximum ridge with 15-element derivative
112
calculate rotation error
114
calculate average signal and background strengths and trace shape on image (a,b,c)
116
calculate contrast and displacement errors (a,b,d)
122
find maximum correlation (a,b)
124
calculate average signal and background strengths and trace shape on image (a,b,c)
calculate contrast and displacement errors (a,b,d)
126
128
find maximum correlation (a,b,c)
130
check constraints for other specks
132
calculate average signal and background strengths and trace shape on image (a,b,c)
134
calculate contrast and displacement errors (a,b,d)
118
test p(contrast(a,b) | si) > Ct ? for shape(a,b,c) visibility and determine ACR passing
120
generate contrast / visibility / ACR-passing rate and displacement errorreports
Stop

FIG. 8

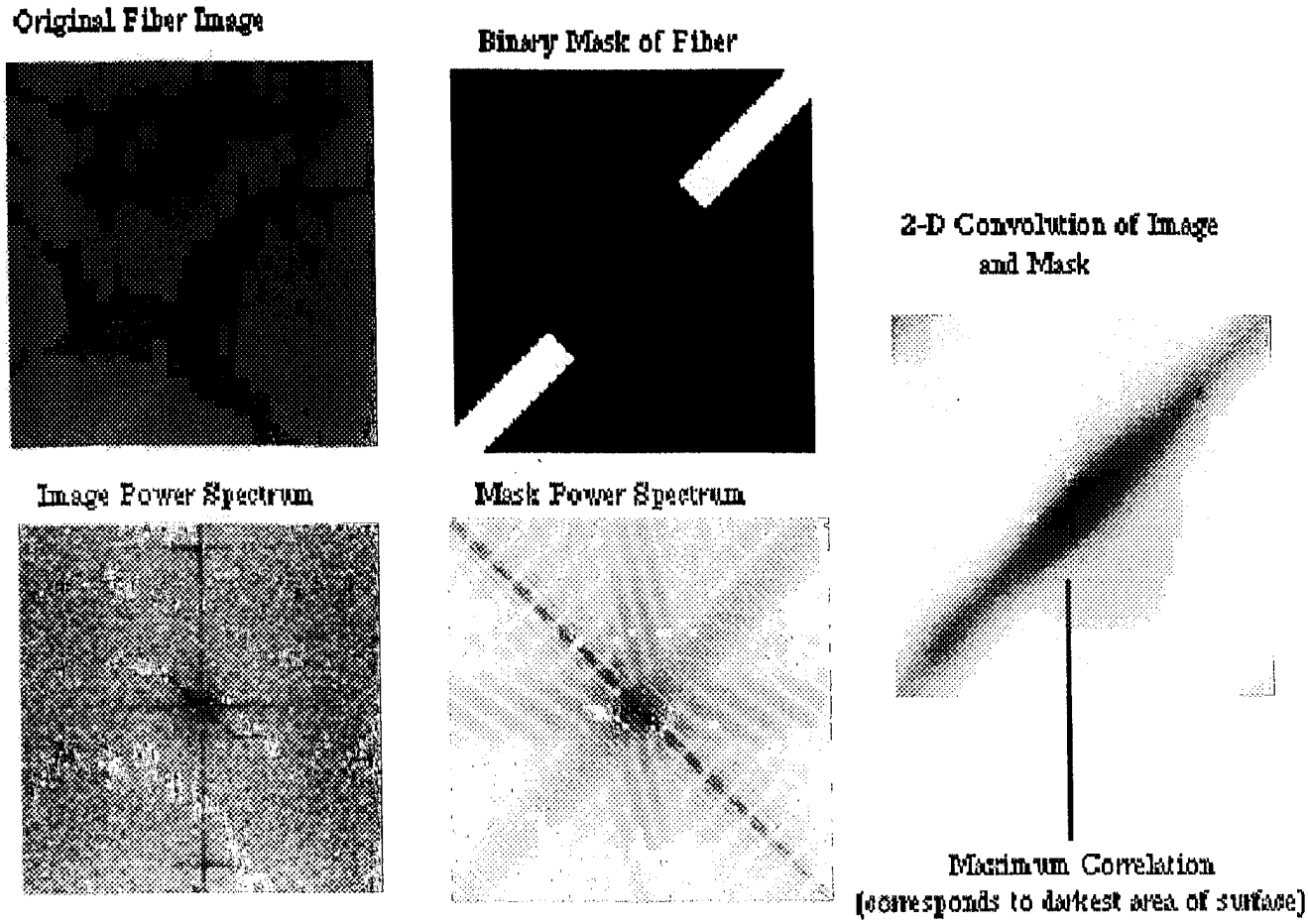
Original Fiber Image
Binary Mask of Fiber
2-D Convolution of Image and Mask
Image Power Spectrum
Mask Power Spectrum
Maximum Correlation
(corresponds to darkest area of surface)

FIG. 9

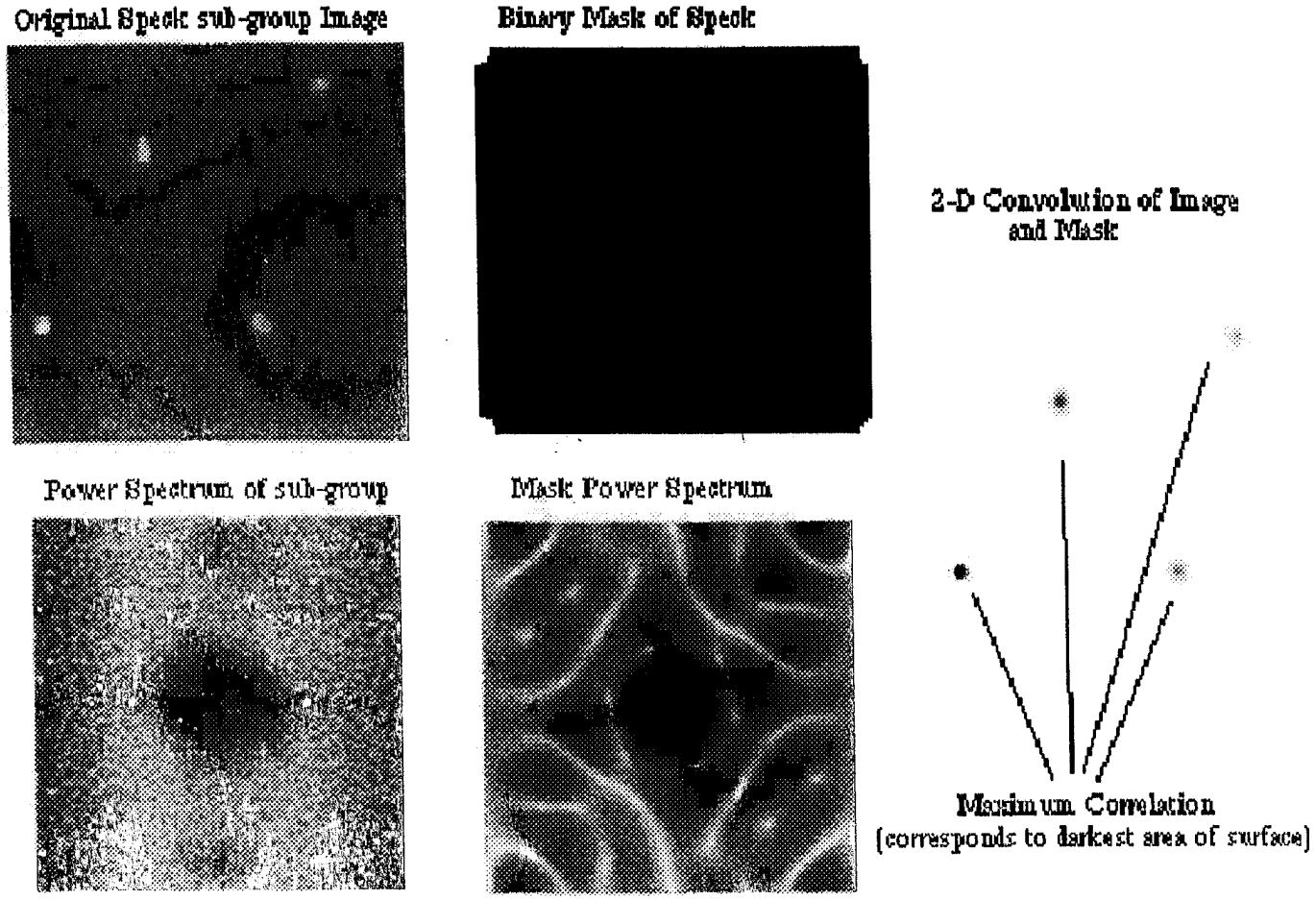
Original Speck sub-group Image
Binary Mask of Speck
2-D Convolution of Image and Mask
Power Spectrum of sub-group
Mask Power Spectrum
Maximum Correlation
(corresponds to darkest area of surface)

FIG. 10

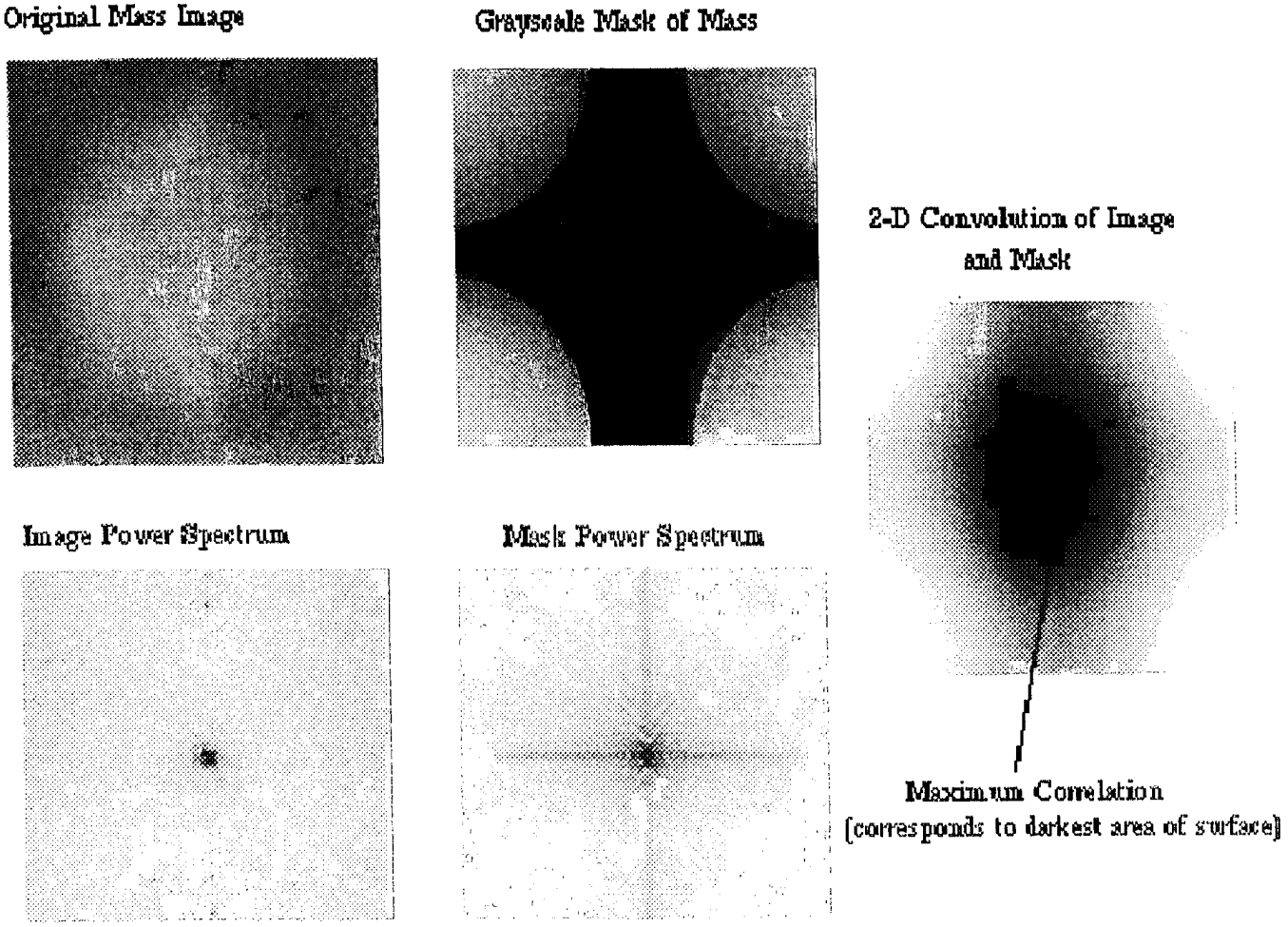
Original Mass Image
Grayscale Mask of Mass
2-D Convolution of Image and Mask
Image Power Spectrum
Mask Power Spectrum
Maximum Correlation
(corresponds to darkest area of surface)

FIG. 11

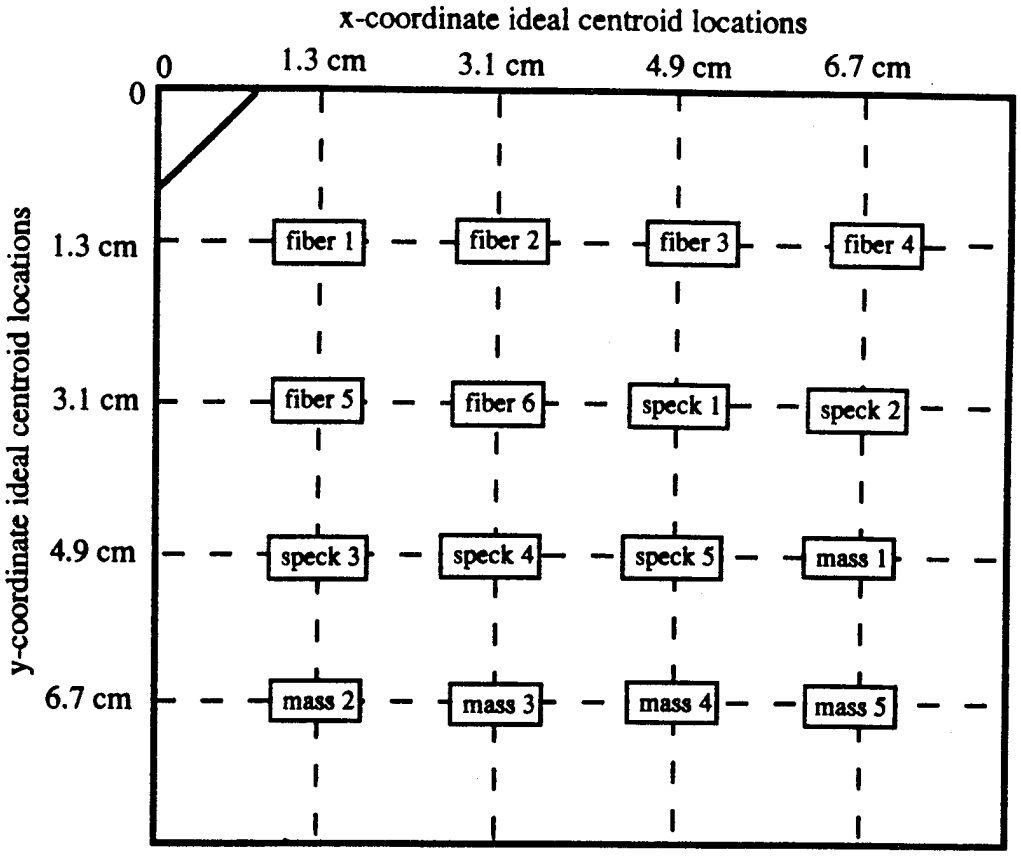
x-coordinate ideal centroid locations
0
1.3 cm
3.1 cm
4.9 cm
6.7 cm
y-coordinate ideal centroid locations
0
1.3 cm
3.1 cm
4.9 cm
6.7 cm
fiber 1
fiber 2
fiber 3
fiber 4
fiber 5
fiber 6
speck 1
speck 2
speck 3
speck 4
speck 5
mass 1
mass 2
mass 3
mass 4
mass 5

FIG. 12

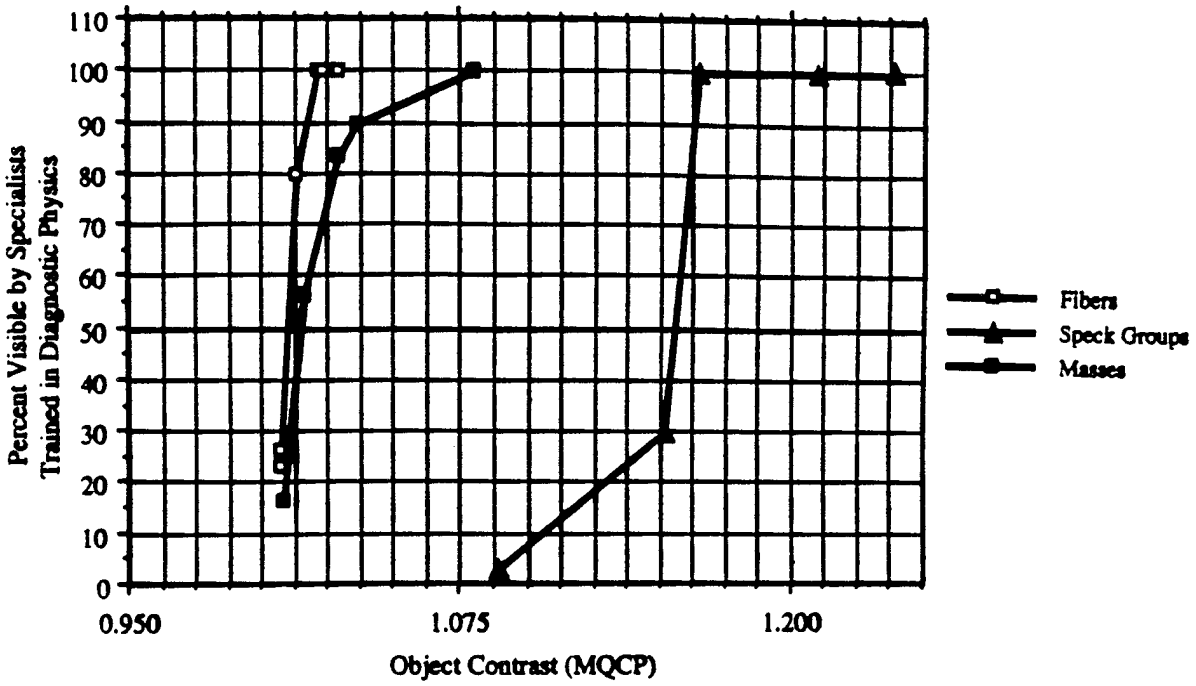
Percent Visible by Specialists Trained in Diagnostic Physics
110
100
90
80
70
60
50
40
30
20
10
0
0.950
1.075
1.200
Object Contrast (MQCP)
Fibers
Speck Groups
Masses

FIG. 13

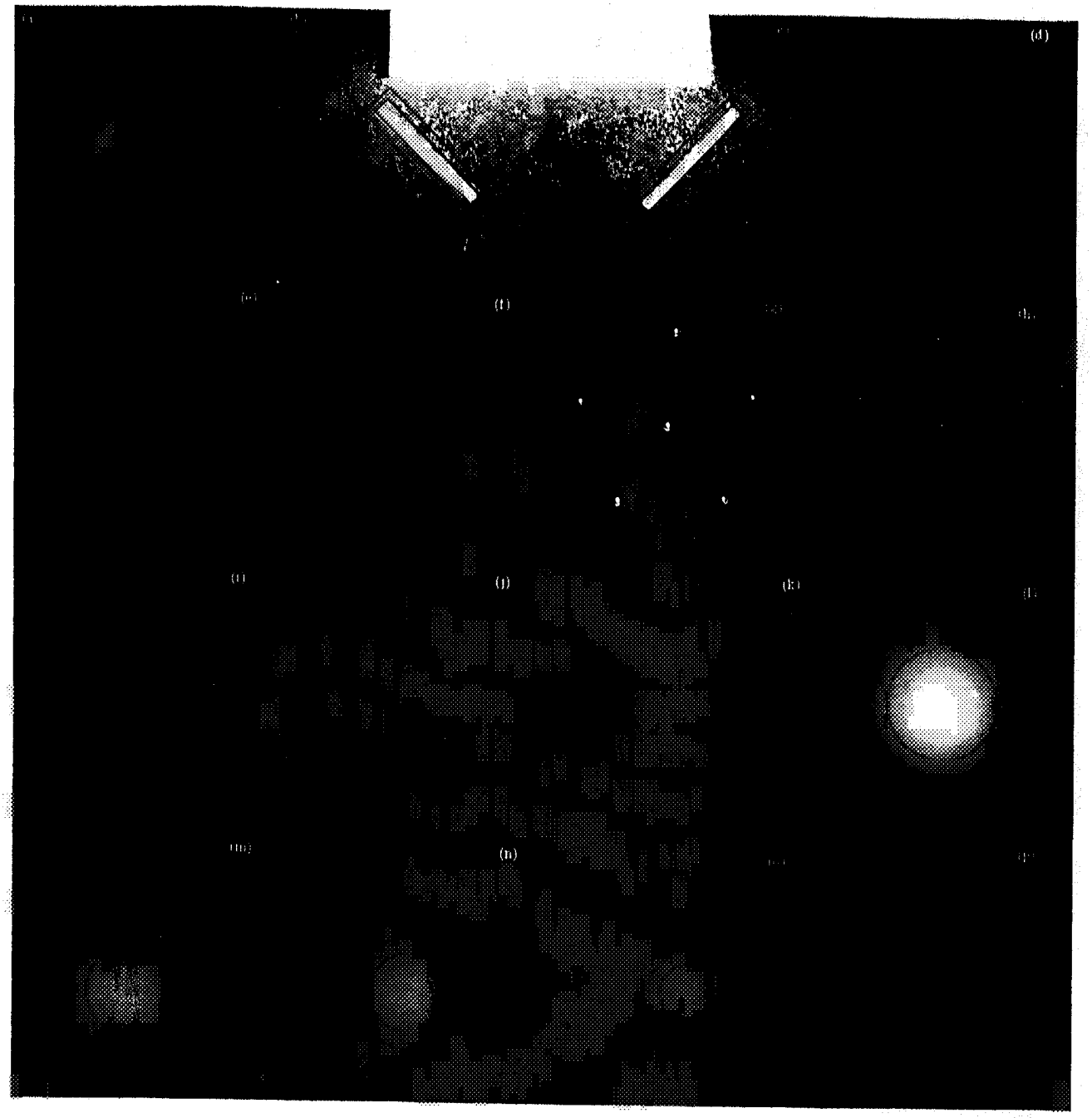

FIG. 14

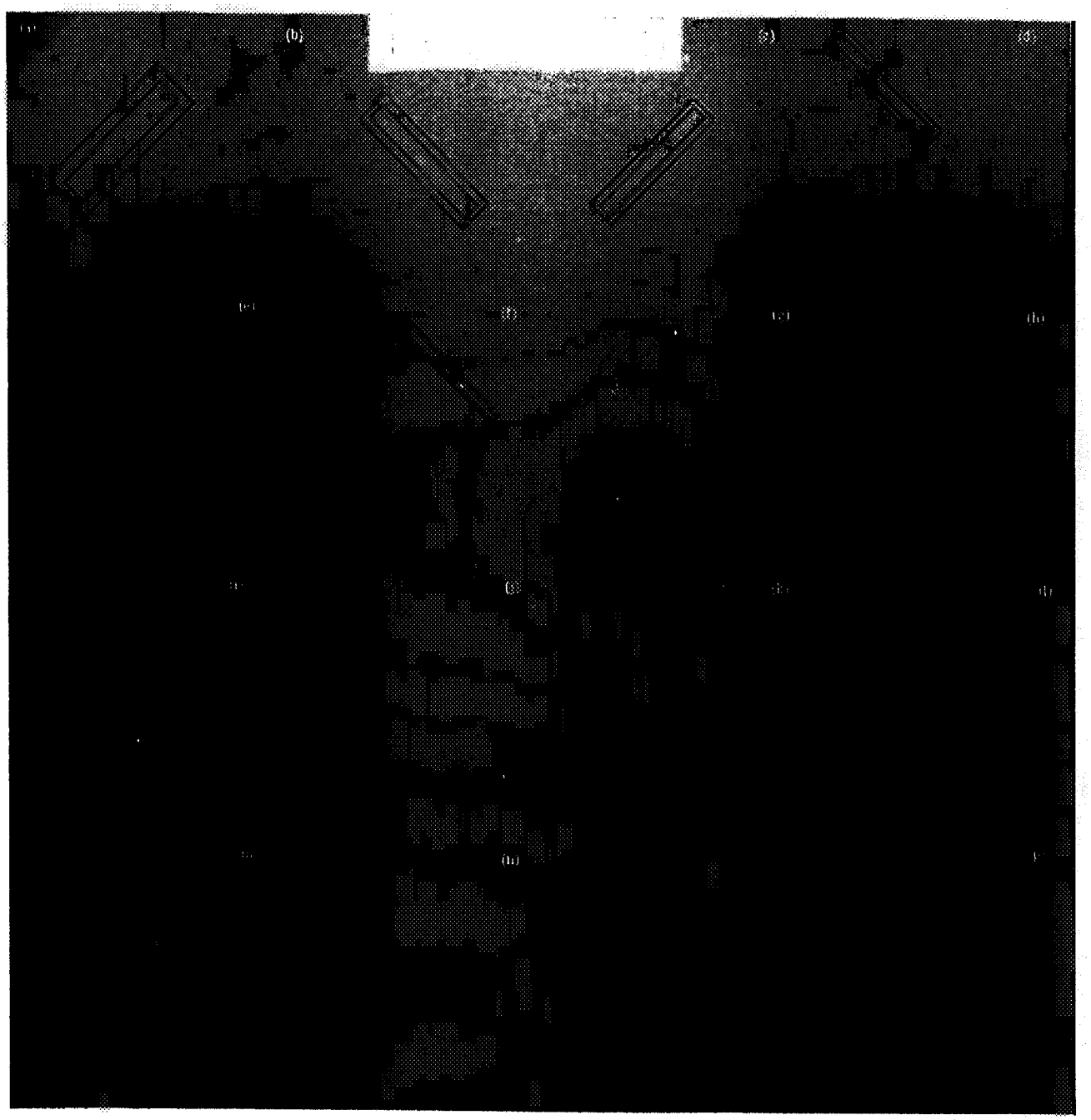

FIG. 15

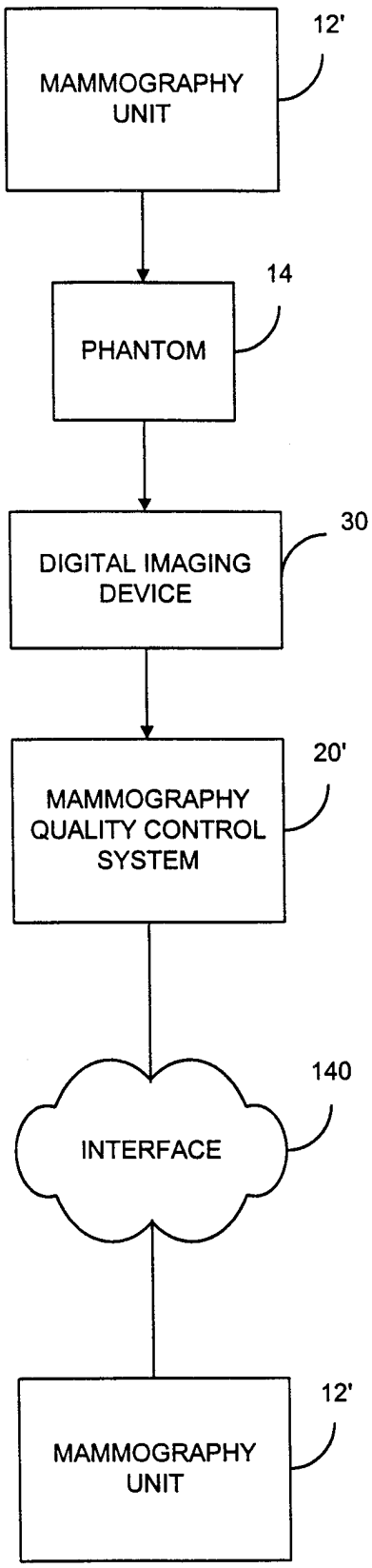
MAMMOGRAPHY UNIT
12'
PHANTOM
14
DIGITAL IMAGING DEVICE
30
MAMMOGRAPHY QUALITY CONTROL SYSTEM
20'
INTERFACE
140
MAMMOGRAPHY UNIT
12'

FIG. 16